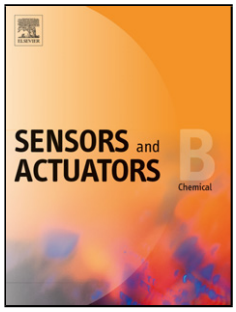


Title: Zonal Selectivity by Sensitivity Modulation in Linear Tetrapolar Impedance Sensors

Authors: Fabián N. Moretti, Jorge L. Cabrera, Rossana E. Madrid

PII: S0925-4005(17)31538-1
DOI: http://dx.doi.org/10.1016/j.snb.2017.08.115
Reference: SNB 22982

To appear in: *Sensors and Actuators B*

Received date: 4-4-2017
Revised date: 18-7-2017
Accepted date: 12-8-2017

Please cite this article as: Fabián N.Moretti, Jorge L.Cabrera, Rossana E.Madrid, Zonal Selectivity by Sensitivity Modulation in Linear Tetrapolar Impedance Sensors, Sensors and Actuators B: Chemicalhttp://dx.doi.org/10.1016/j.snb.2017.08.115

# Zonal Selectivity by Sensitivity Modulation in Linear Tetrapolar Impedance Sensors

Fabián N. Moretti1,*, Jorge L. Cabrera1 and Rossana E. Madrid2,3

1 Grupo de Tecnología Biomédica (GTB Group), Universidad Tecnológica Nacional, Facultad Regional Avellaneda (UTN-FRA), Bs.As., Argentina.

2 Instituto Superior de Investigaciones Biológicas (INSIBIO), CONICET, San Miguel de Tucumán, Argentina.

3 Laboratorio de Medios e Interfases (LAMEIN), Departamento de Bioingeniería, Facultad de Cs. Exactas y Tecnología, Universidad Nacional de Tucumán, San Miguel de Tucumán, Argentina.

*Correspondence to: Fabián N. Moretti, Universidad Tecnológica Nacional, Facultad Regional Avellaneda (UTN-FRA). Campus Villa Domínico, Ramón Franco 5050 (1874). Villa Domínico, Bs.As., Argentina.

E-mail: fnmoretti@fra.utn.edu.ar, fnmoretti@gmail.com

## Graphical abstract

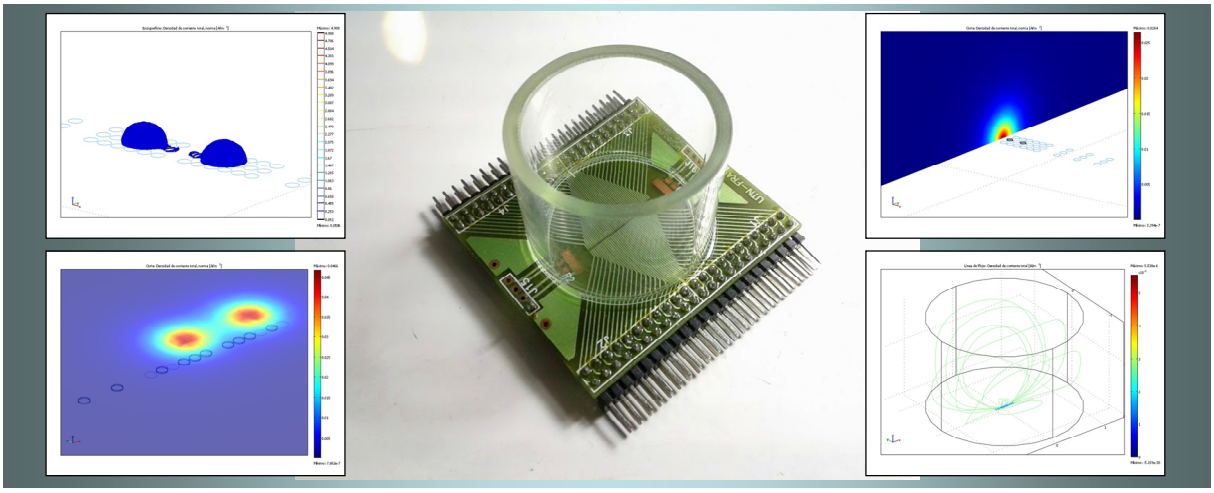

*"Zonal Selectivity by Sensitivity Modulation in Linear Tetrapolar Impedance Sensors"* paper highlights:

Highlights

- Novel approach for designing tetrapolar impedance sensors based on analyzing maximum sensitivity curves
- A complete theoretical and FEM model sensitivity analysis for linear tetrapolar sensors is proposed
- Sensitivity maps and maximum sensitivity curves over critical zones of the sensor were obtained
- The analysis shows that it is possible to have zonal selectivity by means of sensitivity modulation changing the electrode position

Keywords: sensitivity; tetrapolar measurement; impedance sensors; MEA; Mems; EIS;

## 1. Summary

This work investigates the behaviour of a tetrapolar impedance sensor due to sensitivity issues caused by inherent method measurement when inter-electrode spacing is changed. Finite Element Method (FEM) modelling of the sensitivity spectra was computed to analyse maximum sensitivity levels in desired zones of the sample and non-common known and unintuitive phenomenon as negative sensitivity lobes inside the sensitivity distribution field. Sensitivity maps as a function of electrode position were obtained and maximum sensitivity curves were extracted to identify the best configuration for major sensitivity contribution to characterize a specific sample section.

A prototype of a linear tetrapolar sensor array of planar microelectrodes for sensing ionic samples was used for the computational modelling and a brief experimental validation was performed to show the vertical stratification process. The analysis shows that it is possible to have zonal selectivity in the impedance measurement and characterize a desired zone of the sample modulating the sensitivity, changing the electrode position by a scale pattern. This manuscript offers a novel approach for designing tetrapolar sensors based on analyzing maximum sensitivity curves obtained by FEM modelling.

## 2. Introduction

Impedance sensors have been relevant in the last fifteen years due to major benefits offered by an electrical non-invasive, non-destructive and quasi-real time sensing methods like Electric Impedance Spectroscopy (EIS) [1-5]. A specific group of Mems, the Micro Electrode Arrays (MEA) are suitable for EIS monitoring in multiply configurations for bio [6-8] and non-bio applications [9-11]. In particular, four electrode measurements offer accurate sample analysis, permitting a specific

sensitivity level for each tetrapolar configuration depending on the relative position of the electrodes in a linear array sensor.

FEM modelling permits an approach to establish the final sensor prototype performance [12-14] and, in this particular case, to recognize and understand the behaviour of the sensitivity distribution as the unique tool capable of showing the phenomenology of a tetrapolar impedance measurement.

In the bibliography and the state of the art, sensitivity maps for a small number of bipolar and tetrapolar arrays were analyzed for certain applications [15-18]. No actions were taken to improve sensor performance using the sensitivity data for better sensor detection.

This work analyzes by FEM modelling a general linear tetrapolar sensor behaviour, using different sets of four electrode measurements. Changing the inter-electrode distance permits a displacement in the sensitivity curve for each measurement. The sensitivity spectra of a tetrapolar measurement is not an intuitive issue, neither can be obtained by practical measurements due to the variation in the global sensitive field that could have positive, zero or negative local values.

As it is further explained in Section 4, the sensitivity field depends on the relative position of the electrodes, defining a lead field value at each point of the sample under study. Only an analytical study using FEM modelling can explain the behaviour of the leads for a selected point in the sample where the impedance wants to be measured.

The simplified electric analysis done in this work is useful to understand tetrapolar sensor overall performance as the result of zonal interaction due to sensitivity issues. Finite Element Modelling was used to characterize the sensitivity spectra obtaining detailed maps for analysis. Maximum sensitivity curves extraction from sensitivity maps creates a powerful tool in sensor applications. Maximizing the sensitivity over specific regions within the volume of the sample serves as a novel method for sensor designing.

# 3. Numerical Modelling

## 3.1. Model Generalities

The model recreates a microelectrode array (MEA) platform for EIS analysis (Fig. 1). In this particular case, the sensor prototype was designed to measure ionic samples.

The MEA has different sets of four electrodes called steps (S1 to S7) to analyze the sample (Fig. 2). Each step changes the inter-electrode spacing to perform the impedance measurement as shown in Table 1.

The numerical 2D model is composed by a sample container, with a conducting medium as the sample dummy and the sensing electrodes to perform the measurement. The container is represented as a

non-conducting rectangle (30x35mm) with planar metal electrodes (200µm of diameter) at the bottom (*x-axis*). The medium was considered homogeneous and pure resistive of known conductivity, emulating the ionic sample (Fig. 3).

### 3.2. Model assumptions and initial conditions

A simplified electrical pure resistive computational model is proposed to describe the behaviour of the sensitivity field as an initial approach to improve sensor performance. The model consists in calculating the sensitivity (Section 4.3, Eq. 1) for a selected current in a desired medium. The sensitivity field was modelled over a homogeneous resistive medium (NaCl with 1.4 S/m) for a chosen injecting current.

The FEM model was calculated for analyzing small current behaviour, despising frequency effects. Due to complex non linear effects occurred with high amplitude signal applied to a non-linear system like an electrode/medium interface [19-20], the analysis focuses on characterizing the sample as better as possible without disturbances.

Material parameters in the simulation were standard and taken from the library (i.e., for the acrylic sample container and the gold metal electrodes). For calculations, the model was simulated with the AC/DC module, using in-plane currents, in steady state (Comsol Multiphysics).

Accurate mesh generation with triangular elements was used for the domains medium and electrodes (Fig. 3). Additional mesh refinement in critical medium-electrode boundaries was applied for detailed results. A linear solver (UMFPACK) was used for a steady state FEM solution with automatic matrix symmetry.

### 3.3. Electrical configuration. Current Injection

Basic tetrapolar EIS measurement consists of injecting a signal of known characteristics of amplitude and frequency over the current electrode pair and registering the potential changes over the voltage electrode pair.

Current injection was applied over the selected current electrode pair, setting the $I_+$ electrode as source and the *I*- electrode as drain (setting zero volt potential). For the sensitivity field calculus, only the current electrodes are taken into account and for this particular sensor application, the outsider electrodes were always the current electrode pair for every selected step.

## 4. Mathematical model

### 4.1. Lead field basis

Lead field theory was originally developed for the study of electrical dipole sources in a bounded volume conductor. A basic analysis can be performed [21] examining the potential field at an arbitrary point *P*, within or at the surface of a volume conductor, caused by an ideal unit dipole (a supposed unit vector) in a fixed location *Q*. Supposing that at the point *P* the potential $\phi P$ due to the unit dipole is *c* (note that the potential at the point *P* is evaluated as usual, relative to another local point or a remote reference point).

Considering now the potential $\phi P$ corresponding to a dipole of arbitrary magnitude *p* is:

$$\phi P = \bar{c}.\bar{p}$$

Any dipole can be resolved in the three-dimensional space into three orthogonal components $p_x$, $p_y$ and $p_z$:

The coefficients $c_x$, $c_y$, and $c_z$ are found as described in Figure 4 by energizing the corresponding unit dipoles at point *Q* along *x*, *y*, and *z-axes*, respectively, and obtaining the corresponding field potentials. Mathematically, the potential $\phi P$ is the scalar product of a vector $\bar{p}$ and the vector $\bar{c}$ (Fig. 5):

The $\bar{c}$ vector is called the *lead vector*. The lead vector is a three-dimensional transfer coefficient which describes how a dipole source at a fixed point *Q* inside a volume conductor influences the potential at a point within or on the surface of the volume conductor relative to the potential at a reference location. The value of the lead vector depends on the location *Q* of the dipole $\bar{p}$, the location of the field point *P*, the shape of the volume conductor and the distribution of the resistivity of the volume conductor. The value of the lead vector is a property of the lead and volume conductor and does not depend on the magnitude or direction of the dipole $\bar{p}$.

### 4.2. Lead fields and sensitivity distribution

As for a given field point, the length and direction of the lead vector vary as a function of the source location, for a fixed field point location, there can be assigned to each possible source point the value of the lead vector, establish a lead vector field, which is distributed throughout the entire volume conductor. The lead vector indicates the sensitivity of the lead to the dipole source through the potential. The distribution of the magnitude and the direction of the lead vector is at the same time

the distribution of the sensitivity of the lead to the dipole source as a function of its location and orientation. As it is shown in this paper, sensitivity maps were obtained using lead field theory and from isosensitivity zones maximum sensitivity curves were extracted and plotted in different points of interest for better understanding of the sensor overall performance.

### 4.3. Calculus

Based on the principle of reciprocity and the lead fields theory that characterize sensitivity and energy distribution [22], the sensitivity field of a tetrapolar impedance measurement gives a relation between the measured impedance and its change, caused by a given conductivity distribution. It shows how each region is contributing to the measured impedance signal.

The injected electric current for impedance measurement defines the current density in the volume conductor. The current density is related to the electric field by the conductivity of the volume, which is the reciprocal negative gradient of the potential field. The sensitivity is defined by:

Eq. 1

$$Sens = \frac{\overline{J_V}.\overline{J_I}}{I^2}$$

Where $J_V$ is the current density vector associated to the lead field obtained with energization of the $V+$ and $V-$ electrodes and $J_I$ is the density vector associated to the lead field obtained with energization of the $I+$ and $I-$ electrodes and $I$ the electric current injected.

The sensitivity field is related to the measured impedance as follows:

Eq. 2

$$Z = \int_v \frac{1}{\sigma} \frac{\overline{J_V}.\overline{J_I}}{I^2} dv$$

For constant conductivity $\sigma$, the measured impedance $Z$ is obtained by integrating the volume $v$ under analysis [15, 21]. The equation gives the contribution from the volume to the total measured impedance and the dot product expresses the sensitivity to conductivity changes throughout the entire volume conductor.

It is important to take into account that the result of the sensitivity calculus is a scalar field, it could be positive or negative depending on the orientation of the two lead fields. Therefore, the measured impedance may increase, decrease or remain unaffected due to conductivity changes in a particular region. A zonal increment of resistivity in a region of negative sensitivity produces a decrement in

the total measured impedance. This undesired effect is not noted during normal sensor measurement but is always present.

# 5. Post processing Analysis

### 5.1. Sensitivity Spectra

The sensitivity distribution was obtained by computing the sensitivity on a 2D plane and plotting the results as a map for every set of four electrodes. The values of sensitivity can vary from positive, zero, to negative and indicate how the zonal sensitivity influence affects the entire sensor performance (Section 9.1, Figure 7 and 8).

### 5.2. Maximum Sensitivity Curves

From the sensitivity spectra, maximum sensitivity curves can be obtained to identify for a selected region which tetrapolar set of electrodes has better sensitivity contribution to characterize a specific sample section. Post processing the FEM data, selecting a desired depth of penetration (distance *h* from electrode plane), maximum values were obtained by maximizing the sensitivity function and constructing a maximum vector. This procedure is repeated for every electrode set until maximum sensitivity matrix is achieved (Section 9.2, Figure 9-11).

# 6. Model Dynamics

### 6.1. Electrode Position and Displacement

For a dynamic mapping of the sensitivity gradient as a function of the electrode position (Section 3.1, Table 1), the electrode placement was changed for the selected step and the FEM model was updated. Static updating was used for each electrode step. Boundary conditions and coupling variables remain invariant during the process and no other additional changes in local settings were made.

# 7. Experimental validation

As a proof of concept to show the zonal selectivity by means of sensitivity modulation a heterogeneous sample was analyzed. A two layer sample of resistivity ratio 20 to 1 was built for different layer thicknesses. As the sensitivity can be modulated changing the inter-electrode spacing

and the selectivity is shifted depending on the selected electrode step chosen, a layered sample with different thicknesses is useful to show maximum detection levels for each electrode step. This process characterizes the sample by vertical stratification.

### 7.1. Layers building for different thicknesses and steps

Sample emulation was made using gels to recreate a two layers sample. A white gel with resistivity of 200kΩ.mm and a transparent gel with resistivity of 10kΩ.mm were used.

For a fixed height of the volume container $h_c$, the first layer was made with the white gel of thickness $h_w$ and the second layer was made with the transparent gel of thickness $h_t$ completing the container up to the maximum thickness $h_c$. The white gel was increased by discrete steps to form the sample sets and the container was completed with transparent gel as necessary.

Five stratified samples of two layers were built (Table 2). For each thickness $h_w$, impedance measurements were taken.

For each sample analysis, impedance measurements were performed for the seven electrode steps *S1* to *S7*. Experimental impedance measurements were performed with a Solartron 1250/1287 system (See Section 9.3, Fig. 12). For a selected electrode set, at a fixed current intensity of 5μA and frequency of 1kHz injected, the impedance was registered. For each step, five measurements were taken and averaged, then the impedance value was used to compute the apparent resistivity value and the result was plotted.

The apparent resistivity $\rho$ can be determined by the following $\rho = k.Re(Z)$, where $k$ is the coefficient of proportionality defined by several parameters as electrode size, relative electrode position and geometrical form and size of the medium. For the analyzed case, all these parameters are constant and only the electrode position is variable. The coefficient of proportionality of the array is defined by $k_{Sn} = 2.\pi.a$, where $a$ is the inter-electrode distance (Section 3.1, Table 1).

Finally, in the analysis of the family of curves, the comparison was made with the value of resistivity for the same step between the five stratified samples to detect changes in the measured resistivity that correlates with thickness changes.

## 8. Plotting and Graphs

Maximum sensitivity maps were plotted to show sensitivity distribution for every step (Fig. 7 and 8). Plots of maximum sensitivity curves are shown in different zones of interest and different penetration depths, over sensing electrodes, at half distance of the sample container and near the top of the container, to show sensitivity changes (Fig. 9-11). For the experimental validation, apparent resistivity values obtained using sample stratification method were plotted (Fig. 13).

# 9. Results and Discussion

## 9.1. Sensitivity Maps

Sensitivity maps are shown in the Figure 7.a to 7.g, corresponding to the sensitivity field for each electrode step. There can be seen regions of different sensitivity conforming lobes due to current density distribution. The sensitivity gradient changes in magnitude and direction as a function of electrode position.

In specific zones, sensitivity shows a negative value and for the specific tetrapolar configuration used, the negative lobe is placed between current and voltage electrode, as can be seen in detail in Figure 8.

The FEM analysis brings relevant information about electrodes behaviour that could not be obtained by practical methods or measurements.

## 9.2. Maximum Sensitivity Curves

Maximum sensitivity curves are shown in Figure 9 to 11, corresponding to maximum sensitivity for each electrode step in different zones of interest for the EIS sensor, as follows:

### 9.2.1. Maximum sensitivity curves over current electrode surface

Over the current electrode surface ($h$=0), values ranges for each step are positive. It can be seen clearly in the sensitivity maps and corroborated with the maximization process.

### 9.2.2. Maximum sensitivity curves between voltage and current electrodes

Between voltage and current electrodes, as it was described in the plotted maps, negative sensitivity values are present. This is a zone of particular interest for this phenomenology. It can be seen the negative zones occur near the voltage electrodes, where detection zones are present in impedance sensors.

### 9.2.3. Maximum sensitivity curves at selected heights from the electrode plane

Maximum sensitivity values were extracted at four heights from the electrode plane ($h$=0mm, $h$=1.2mm, $h$=12mm and $h$=24mm) to show changes in the local sensitivity over the total measured volume.

In the Figure 11.a., maximum sensitivity is shown over the electrode surface plane ($h$=0mm) for every electrode step. In the Figure 11.b., near the electrodes surface ($h$=1.2mm), maximum sensitivity oscillates between voltage and current electrodes corresponding to overlapped sensitivity lobes in the negative zones, shown in the previous maps. In the Figure 11.c., ($h$=12mm) it is clearly seen that every electrode step has its own characteristic sensitivity curve, increasing the detection from step 7 to 1. This analysis is useful to establish for a selected penetration depth, which electrode configuration improves the measure. For this particular case, the electrode step 4 averages the detection, which is neither done by the step 1, which has major sensitivity in the centre but decreases in the periphery, nor by the step 7, which has low detection levels in the entire span.

Finally, far from the electrode plane ($h$=24mm), the sensitivity distribution tends to be more homogeneous (Fig. 11.d.). It can be seen each electrode step has flatten out its own sensitivity curve and maintains the order in the stack from step 7 to 1.

## 9.3. Experimental Results

The experimental setup used for the impedance measurements is shown in Figure 12.

Apparent resistivity values obtained using sample stratification method are plotted in Figure 13, for the five analyzed samples for the seven impedance scanning points values per sample. Experimental

parameters are 5µA, @1kHz of exploratory current (*Re(Z)* only considered) and the reference temperature of 25˚C, as explained in Section 7. Values were converted to apparent resistivity and plotted as a function of the electrode spacing. Error bars are shown for each step.

It can be seen in Figure 13 that the five samples (*w1-w5*) form a family of curves with an origin of similar resistivity in the *S7* step (closer electrode spacing *Smin*) and splitting up until the *S1* step (*Smax)*, describing a stack due to the changes in the thickness of the first layer $h_w$. This phenomenon can be understood by analyzing the increment of $h_w$, step by step.

Beginning with the layer *w1* with $h_w$ = 2.50mm, both *S7* and *S6* steps measure a similar resistivity. Also for the rest of the layers *w2-w5*, the value of resistivity does not vary more than 5% between these two steps. This characteristic can be explained through the concepts of sensitivity and maximum penetration depth of a sensor step.

When comparing the different layers *w1-w5*, the resistivity for *S7* and *S6* shows minimal values in all the layers, because the maximum sensitivity penetration depth for both steps is under the adopted layers height $h_w$. For this reason, the tetrapolar steps *S7* and *S6* cannot register increments in the layer thickness for more than 2.50mm.

For the *S5* step, the registered resistivity starts to change significantly from *w1* to *w2*, decreasing for *w3* and maintaining similar values for *w4* and *w5*. The sensitivity for the *S5* gets deeper into the layers thickness registering changes in the resistivity up to *w4* with $h_w$=6.25mm, where the discrimination resolution layers start to diminish.

For the *S4* step, layers discrimination is notorious now for *w1*, *w2* and *w3* with less variation for *w4* and *w5*. The rest of the steps follow the same behaviour, registering resistivity variation when the electrode spacing is increased.

By changing the inter-electrode spacing, it is possible to detect changes in the resistivity at different heights from the electrode array. This sample stratification method is useful to detect changes in the zonal resistivity characterizing heterogeneous samples.

## 10. Conclusions

This work takes advantage of the sensitivity maps, extracting the maximum sensitivity levels for different electrode positions and characterizing the sensor by maximum sensitivity curves for each tetrapolar configuration. This technique can be generalized to any sensor sensitivity analysis to improve overall performance. The sensitivity analysis is mandatory in the design process and it is the

previous stage between sensor design and impedance or electrochemical measurements. Improving the sensitivity of a sensor will lead to better final operating ranges.

Numerical modelling offers a meaningful tool to understand tetrapolar sensor overall performance. Identifying negative sensitivity zones could be crucial in EIS sensors for certain applications, i.e. negative sensitivity zones present over the hybridization zones or recognition sites in chemical or biological applications. In general, tetrapolar impedance sensors offer more reliable sample analysis avoiding intrinsic electrode impedance addition due to contact resistance, but the benefit obtained using this configuration could be minimized for this undesired sensitivity issue.

Over a selected detection zone, establishing which tetrapolar set maximizes the impedance measurement is a major goal for every impedance sensor.

From the sample analysis at different heights from the electrode plane, there can be seen that the range of sensitivity varies from a minimum factor of 2x to a maximum factor of 7x. Choosing the best electrode set could make the difference between proper sample detection and false negatives. Impedance measurements with different electrodes sets forming a linear array offer the advantage of bulk monitoring with the ability of improved resolution in certain zones only changing the inter-electrode spacing, conferring the tetrapolar sensor a new capability, maintaining EIS parameters (current range and frequency) without changing experimental conditions. Maximum sensitivity curves offer full electrode characterization for a correct EIS application of any kind.

**Acknowledgements:** The authors wish to thank Gerardo Battaglia, Edgardo Porral and Roberto Battista for thechnical help and T.P. Mariana Cabrera for editorial support.

# 11. References

1. Guan, J.-G., Y.-Q. Miao, and Q.-J. Zhang, *Impedimetric biosensors.* JOURNAL OF BIOSCIENCE AND BIOENGINEERING, 2004. **97**(4): p. 219-226.

2. Lisdat, F. and D. Schäfer, *The use of electrochemical impedance spectroscopy for biosensing.* Analytical and Bioanalytical Chemistry, 2008. **391**(5): p. 1555-1567.

3. Macdonald, J.R., *Impedance spectroscopy.* Annals of Biomedical Engineering, 1992. **20**(3): p. 289-305.

4. Goster, C.a.C., *Impedance spectroscopy of interfaces, membranes and ultrastructures.* Bioelectrochemistry and Bioenergetics, 1996. **40**.

5. Barsoukov, E. and J.R. Macdonald, *Impedance Spectroscopy. Theory, Experiment, and Applications*, ed. I. John Wiley & Sons, Publication. 2005, Canada.

6. Dorielle T. Price, A.R.A.R., Shekhar Bhansali, *Design rule for optimization of microelectrodes used in electric cell-substrate impedance sensing (ECIS).* 2009.

7. Tang, X., et al., *Carbon Nanotube DNA Sensor and Sensing Mechanism.* Nano Letters, 2006. **6**(8): p. 1632-1636.

8. Nicholas, L.O., et al., *Chronic impedance spectroscopy of an endovascular stent-electrode array.* Journal of Neural Engineering, 2016. **13**(4): p. 046020.

9. Stulík, K., et al., *Microelectrodes. Definitions, characterization, and applications (Technical report).* Pure and Applied Chemistry, 2000. **72**(8): p. 1483-92.

10. Yang, H., et al., *3-D printed adjustable microelectrode arrays for electrochemical sensing and biosensing.* Sensors and Actuators B: Chemical, 2016. **230**: p. 600-606.

11. Fu-Yu, C., et al., *Highly sensitive three-dimensional interdigitated microelectrode for microparticle detection using electrical impedance spectroscopy.* Journal of Physics D: Applied Physics, 2016. **49**(7): p. 075403.

12. Zhu, T. and W. Ye, *Origin of Knudsen forces on heated microbeams.* Physical Review E, 2010. **82**(3): p. 036308.

13. Zhu, T., W. Ye, and J. Zhang, *Negative Knudsen force on heated microbeams.* Physical Review E, 2011. **84**(5): p. 056316.

14. Canali, C., et al., *Bioimpedance monitoring of 3D cell culturing—Complementary electrode configurations for enhanced spatial sensitivity.* Biosensors and Bioelectronics, 2015. **63**: p. 72-79.

15. Grimnes, S., Ø.G. Martinsen, and G.K. Johnsen, *Mutual localization of electrode pairs in a 4-electrode measuring system.* IOP, 2010.

16. Linderholm P., B.T., Vannod J., Barrandon Y., Brouard M., Renaud P., *Two-dimensional impedance imaging of cell migration and epithelial stratification.* Lab on a Chip, 2006. **6**: p. 1155–1162

17. Zu-yao Chang, G.A.M.P., and Gerard C. M. Meijer, *A Comparison of Two- and Four-Electrode Techniques to Characterize Blood Impedance for the Frequency Range of 100 Hz to 100 MHz*, in *IEEE TRANSACTIONS ON BIOMEDICAL ENGINEERING*. 2008.

18. Ma, H., Y. Su, and A. Nathan, *Cell constant studies of bipolar and tetrapolar electrode systems for impedance measurement.* Sensors and Actuators B: Chemical, 2015. **221**: p. 1264-1270.

19. Ruiz, G.A., C.J. Felice, and M.E. Valentinuzzi, *Non-linear response of electrode–electrolyte interface at high current density.* Chaos, Solitons & Fractals, 2005. **25**(3): p. 649-654.

20. McAdams, E. and J. Jossinet, *A physical interpretation of Schwan's limit current of linearity.* Annals of Biomedical Engineering, 1992. **20**(3): p. 307-319.

21. Malmivuo, J. and R. Plonsey, *Bioelectromagnetism , Principles and Applications of Bioelectric and Biomagnetic Fields*. 1995, New York: Oxford University Press.

22. Geselowitz, D.B., *An Application of Electrocardiographic Lead Theory to Impedance Plethysmography.* Biomedical Engineering, IEEE Transactions on, 1971. **BME-18**(1): p. 38-41.

Author Biographies

Fabián N. Moretti was born in Buenos Aires, Argentina. He earned the B.S. degree in Electronic Engineering from Universidad Tecnógica Nacional-FRA, Buenos Aires, Argentina in 2001. In 2010 he earned the MSc. degree in Micro and Nano Electronics from Universidad Autónoma de Barcelona, Barcelona, Spain. He has been with the Universidad Tecnológica Nacional since 2007 engaged in undergraduate teaching and research. He is presently Associate Professor of Electronic Physics at the Universidad Tecnológica Nacional-FRA and the Director of the Biomedical Technology Laboratory (GTB Group) and the Electronic Physics Laboratory at Universidad Tecnológica Nacional-FRA.

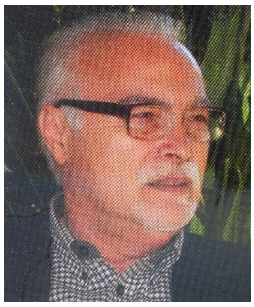

Jorge L. Cabrera was born in Buenos Aires, Argentina. He earned the B.S. degree in Telecommunications Engineering from Universidad Nacional de La Plata, Buenos Aires, Argentina in 1978. He has been with the Universidad Tecnológica Nacional since 1993 engaged in undergraduate teaching and research. He is presently Full Professor of Biomedical Engineering at the Universidad Tecnológica Nacional-FRA and the Director and Researcher at the Biomedical Technology Laboratory, GTB Group, Universidad Tecnológica Nacional-FRA.

Rossana E. Madrid was born in Tucumán, Argentina. She earned the B.S. degree in Electrical Engineering from Universidad Nacional de Tucumán, Tucumán, Argentina in 1991. In 1998 he earned the PhD. degree in Bioengineering from Universidad Nacional de Tucumán, Tucumán, Argentina.She is with Universidad Nacional de Tucumán since 1992 engaged in undergraduate and graduated teaching and research. She is presently Full Researcher at the Mediums and Interfaces Laboratory (Lamein), Universidad Nacional de Tucumán, Tucumán, Argentina.

Figure Caption

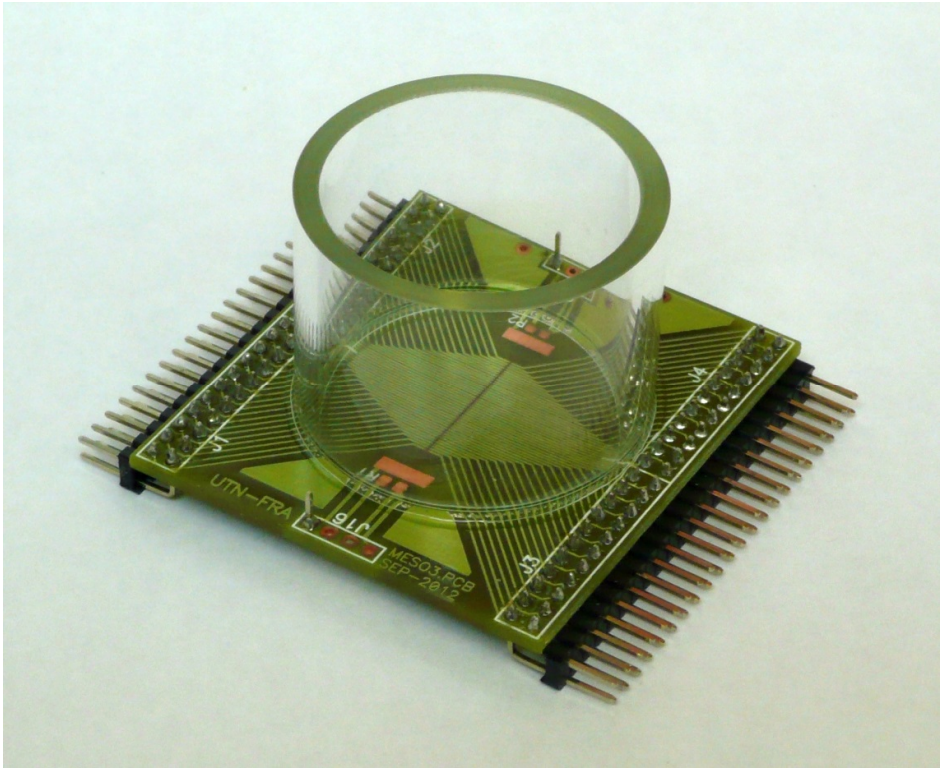


Fig. 1. MEA platform for EIS analysis of ionic samples.

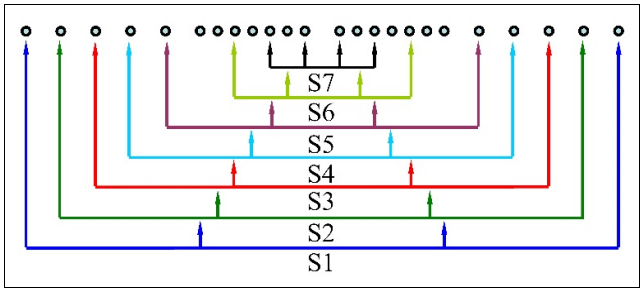


Fig. 2. Sensor array distribution schematic. Top view.

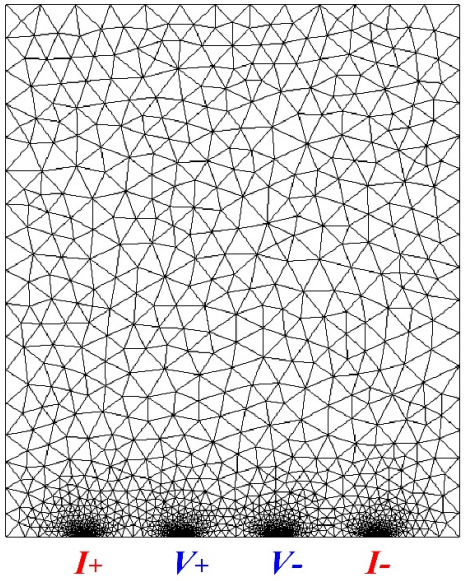


Fig. 3. Mesh tree for the computational calculus. The rectangle represents the sample container with four electrodes at the bottom.

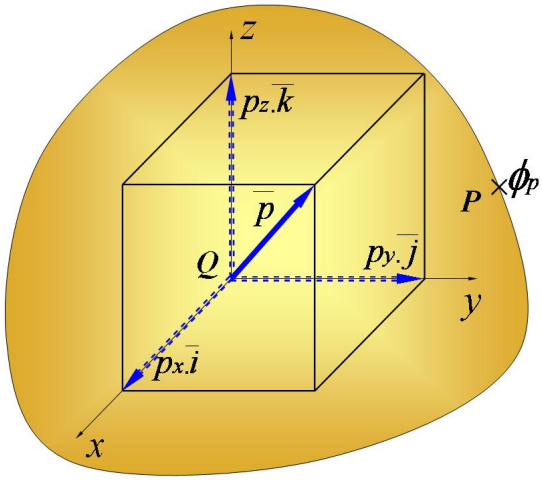


Fig. 4. Schematic of the dipole vector $\bar{p}$ and its components. The three-dimensional proportionality coefficient is called the lead vector $\bar{c}$, where $p = p_x.\bar{i} + p_y.\bar{j} + p_z.\bar{k}$, $\phi P = c_x.p_x + c_y.p_y + c_z.p_z$ and $c = c_x.\bar{i} + c_y.\bar{j} + c_z.\bar{k}$.

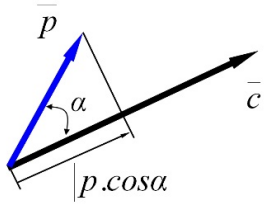

Fig. 5. Schematic of the potential $\phi P$, corresponding to the scalar product of the dipole vector $\overline{p}$ and the lead vector $\overline{c}$, where $\phi P = \overline{c}.\overline{p} = |\overline{c}|.|\overline{p}|.\cos\alpha$.

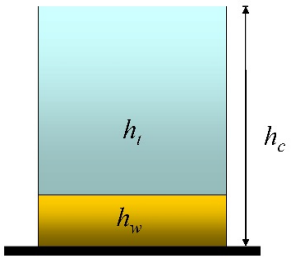


Fig. 6. Schematic of the two layers sample. Where $h_w$ is the thickness of the white gel layer and $h_t$ is the thickness of the transparent gel layer. $h_w + h_t = h_c$ =30mm.

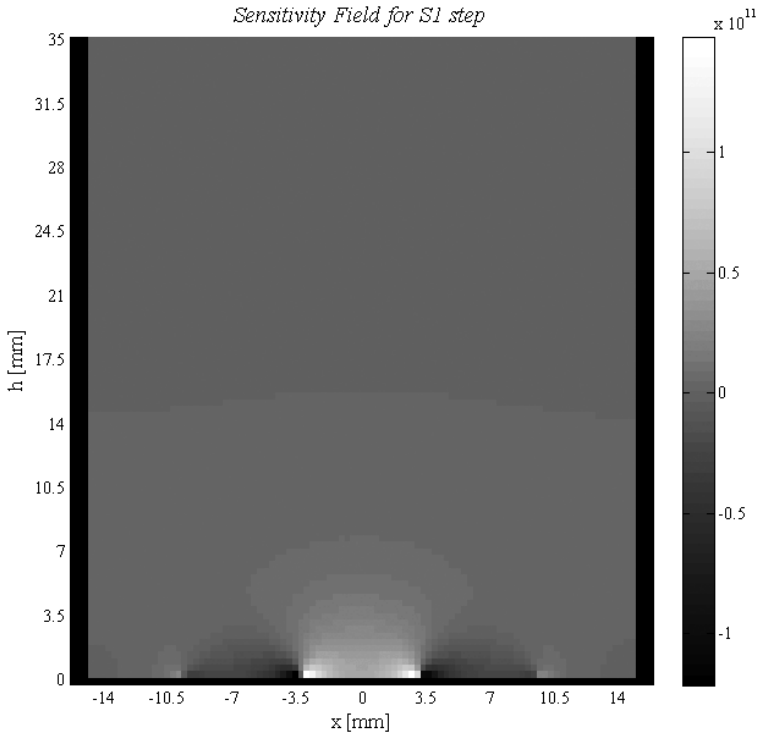


7.a.

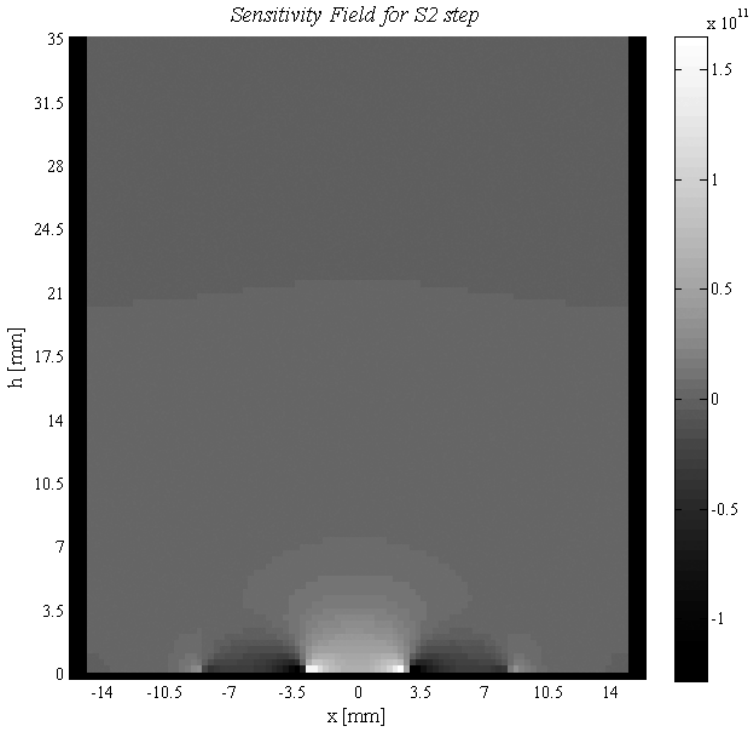


7.b.

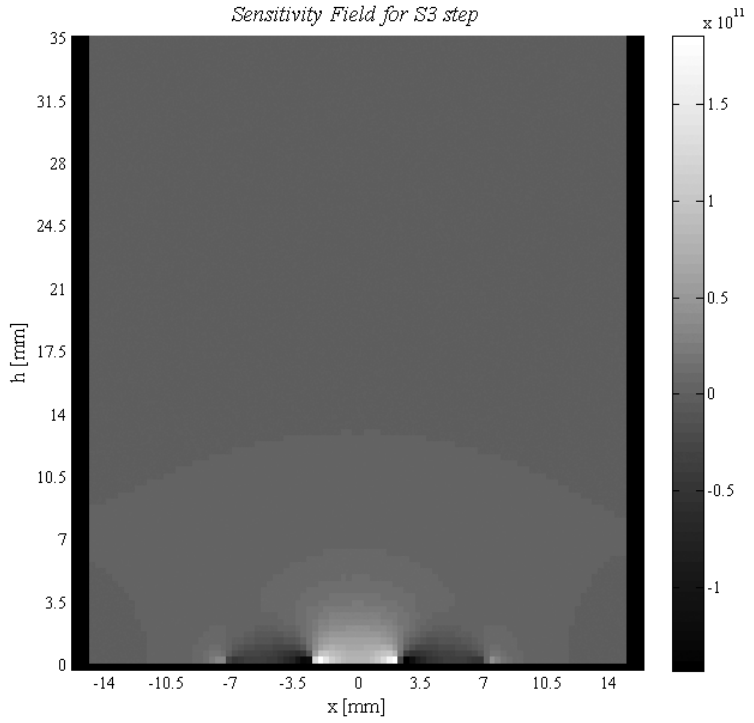


7.c.

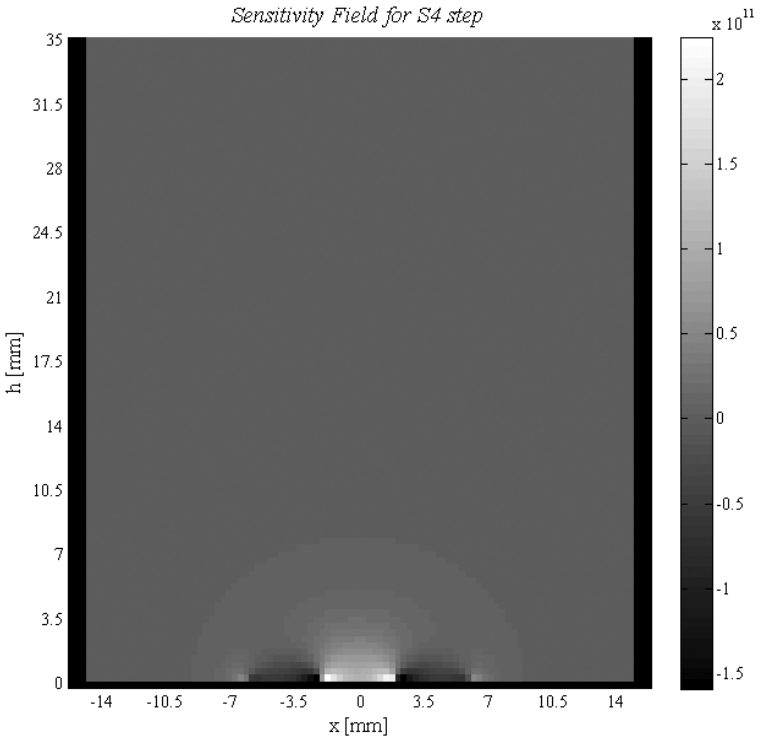


7.d.

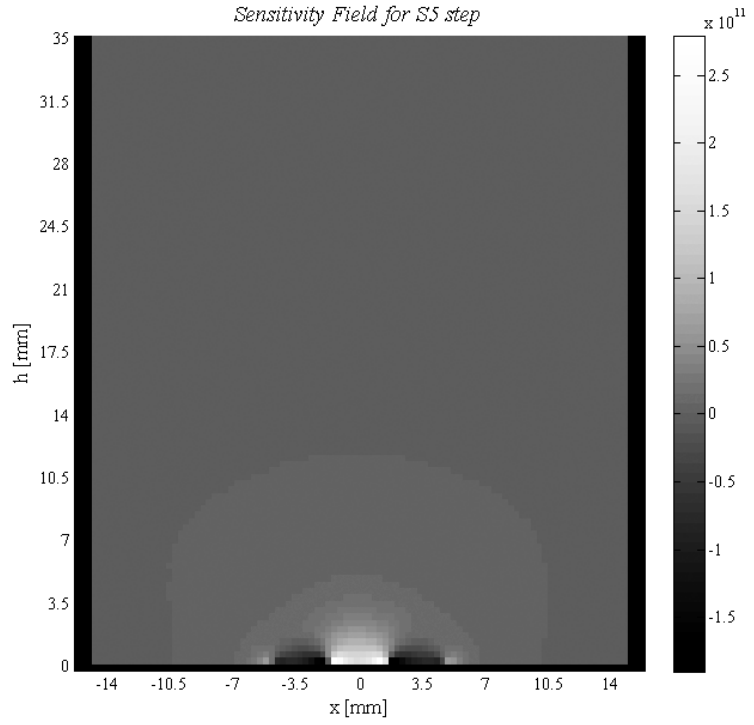


7.e.

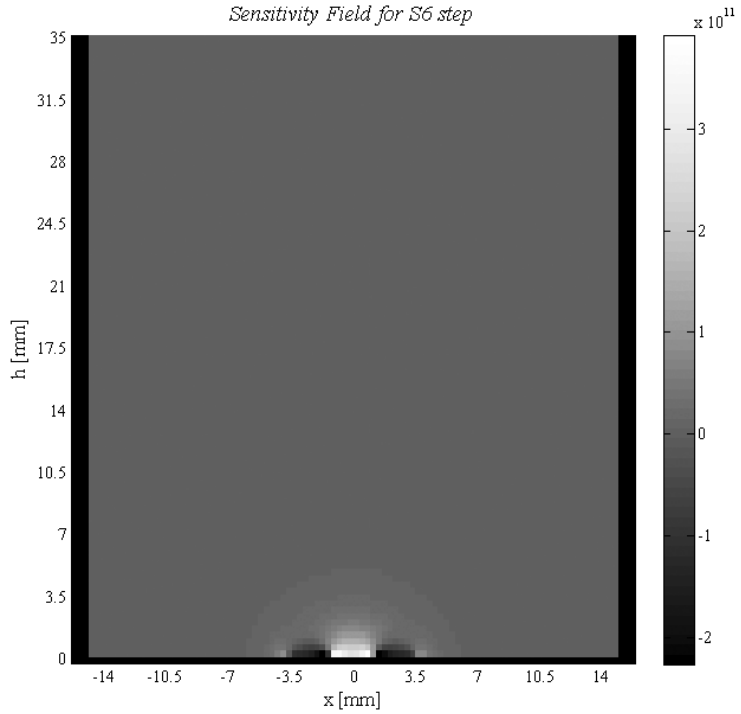


7.f.

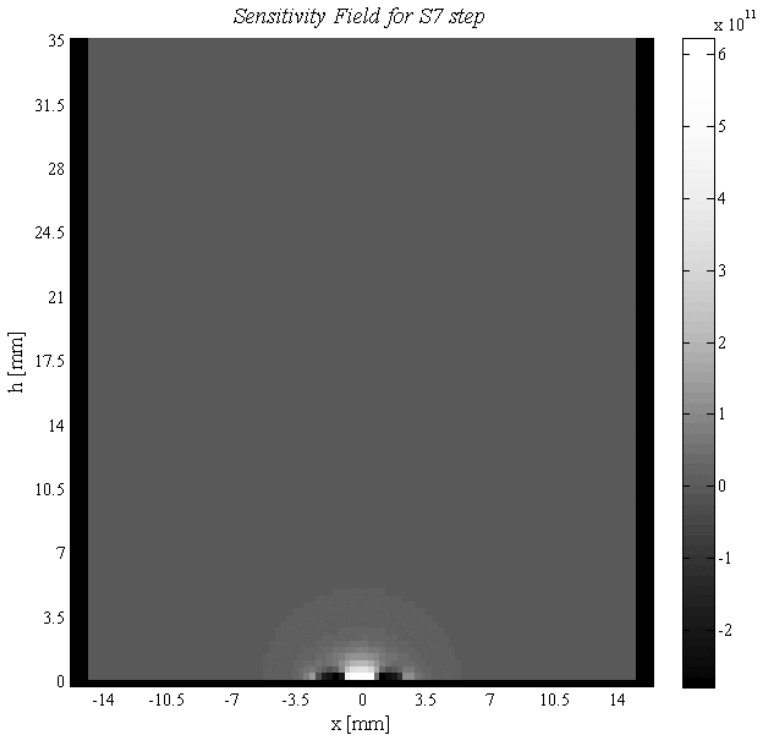


7.g

Fig. 7. Sensitivity Maps for the electrode steps S1 to S7. Sensitivity unit in $1/mm^4$.

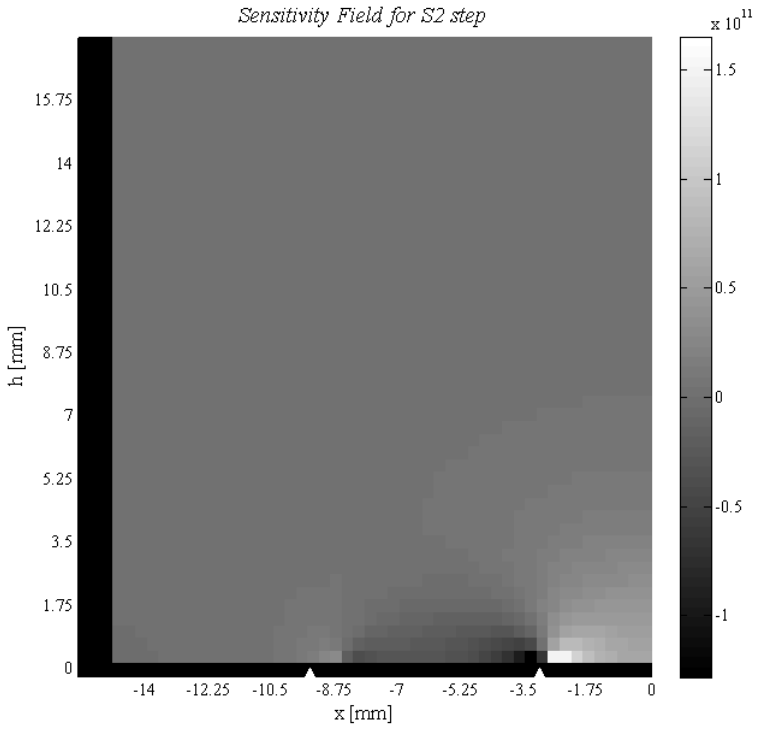


Fig. 8. Zoomed sensitivity field for S2 step for the left half of the array (symmetrical). Negative sensitivity lobe is present between current and voltage electrodes. $I_+$ and $V_+$ electrode position is marked with a white triangle.

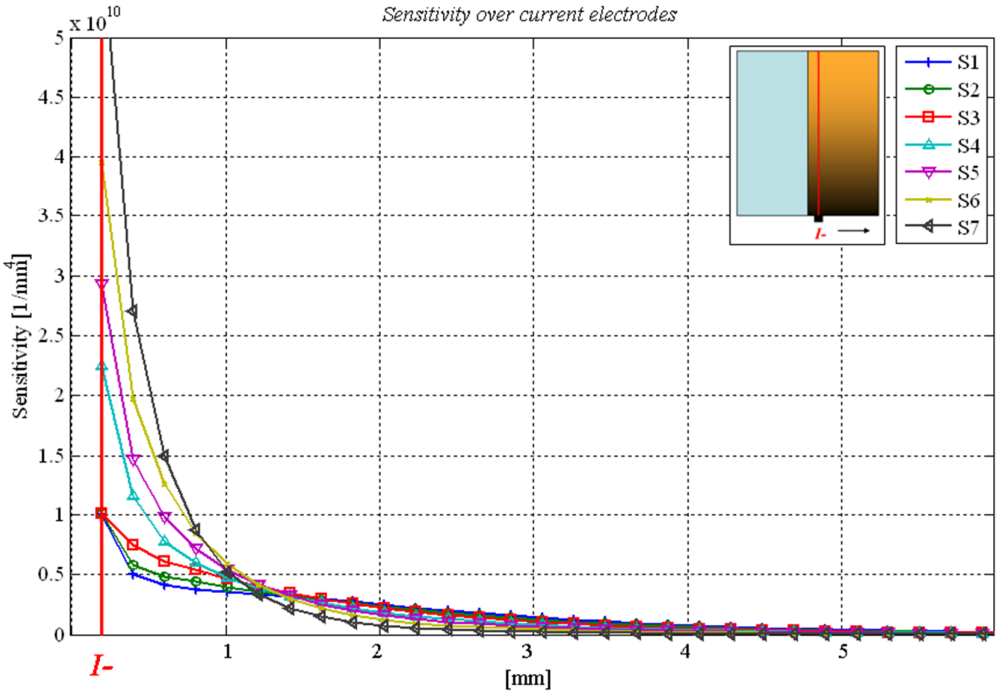


Fig. 9. Maximum sensitivity at *h*=0mm over current electrodes for the right half of the array (symmetrical) for every electrode step. Maximum sensitivity was extracted for every electrode step and superimposed for contrasting purposes. Note that in every step the sensitivity has positive ranges.

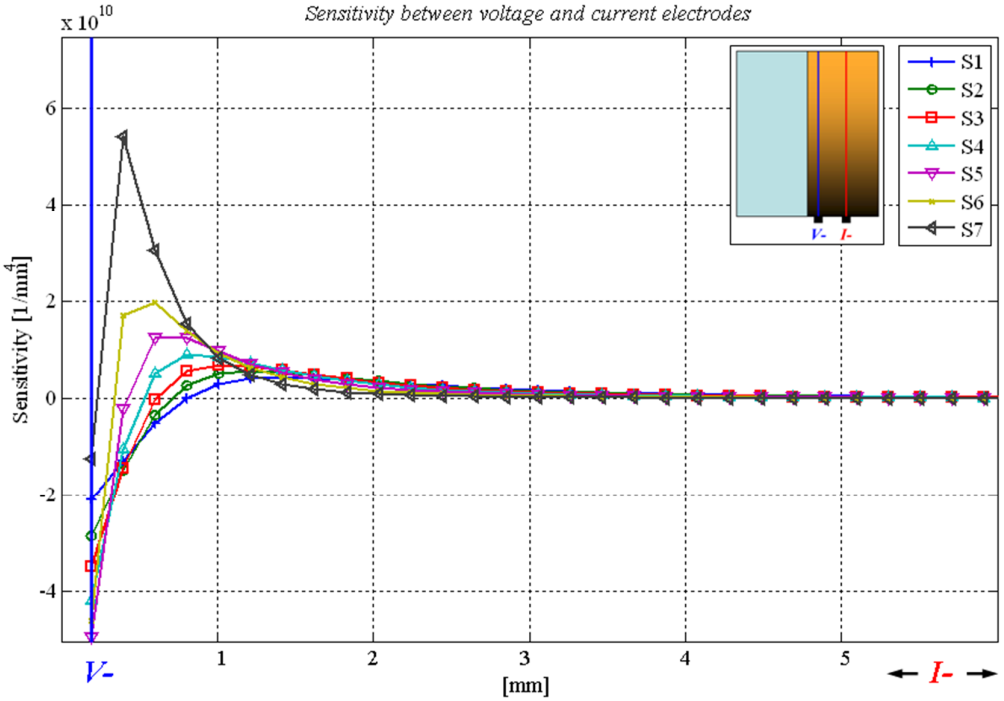


Fig. 10. Maximum sensitivity at $h$=0mm between voltage and current electrodes for the right half of the array (symmetrical). Maximum sensitivity between $V$- and $I$- was extracted for every electrode step and superimposed for contrasting purposes.

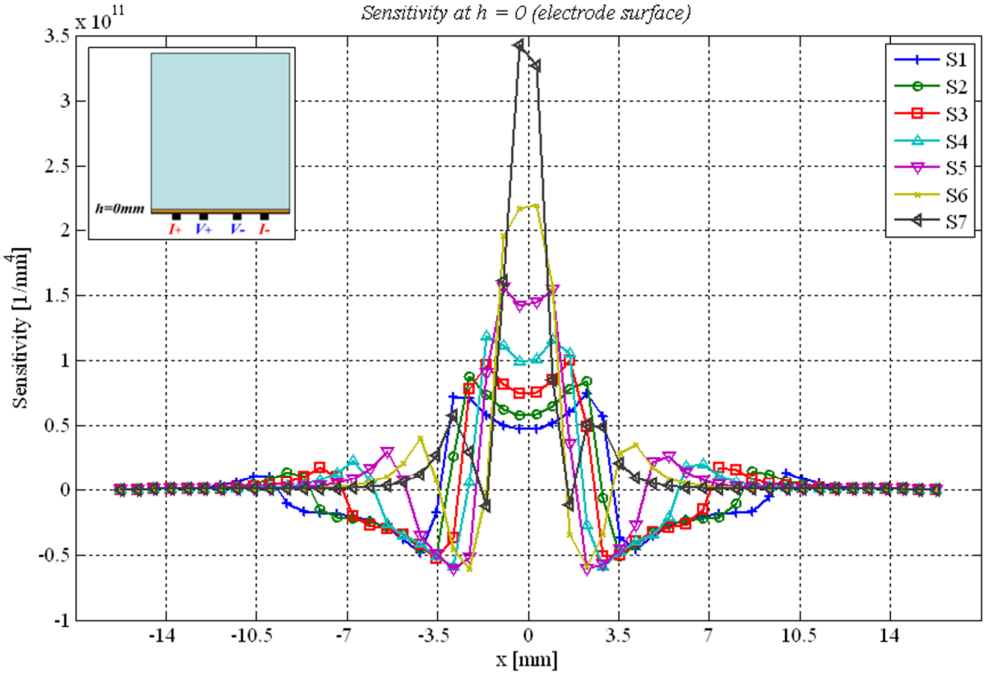


Fig. 11.a. Maximum sensitivity at *h*=0mm for every electrode step.

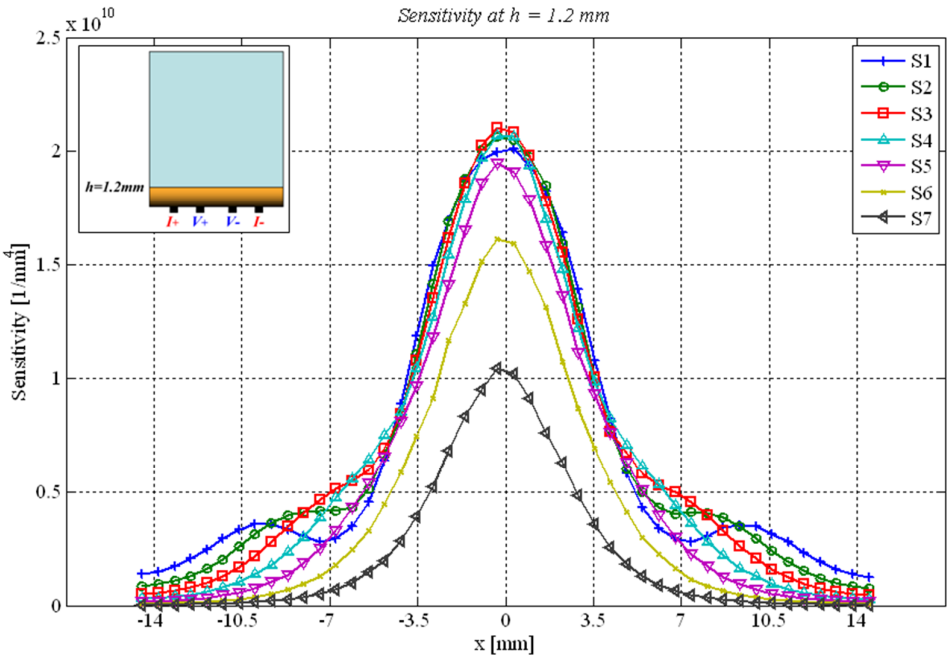

Fig. 11.b. Maximum sensitivity at *h*=1.2mm for every electrode step.

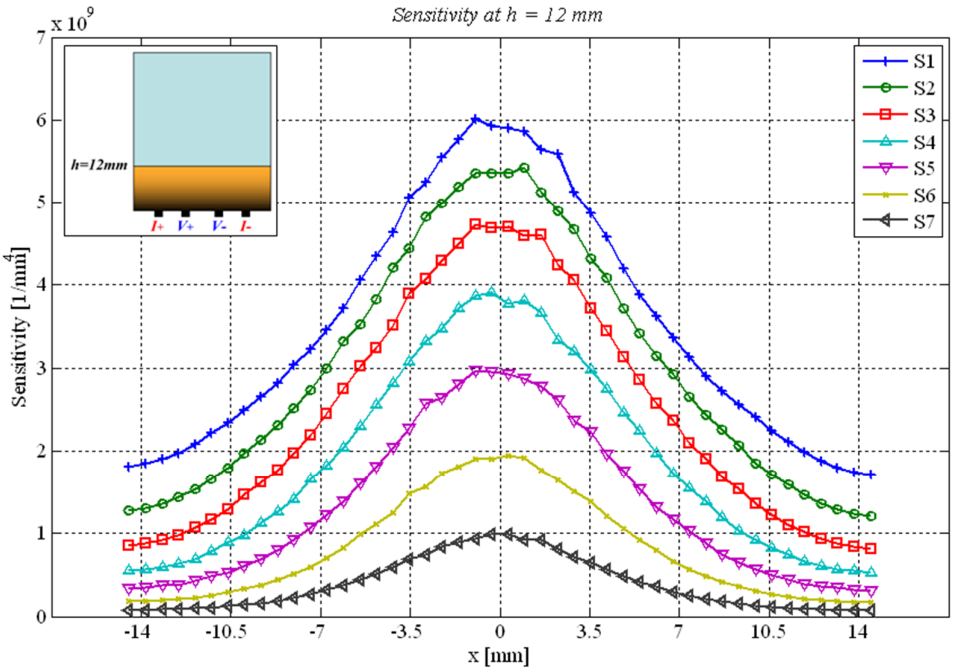


Fig. 11.c. Maximum sensitivity at *h*=12mm for every electrode step.

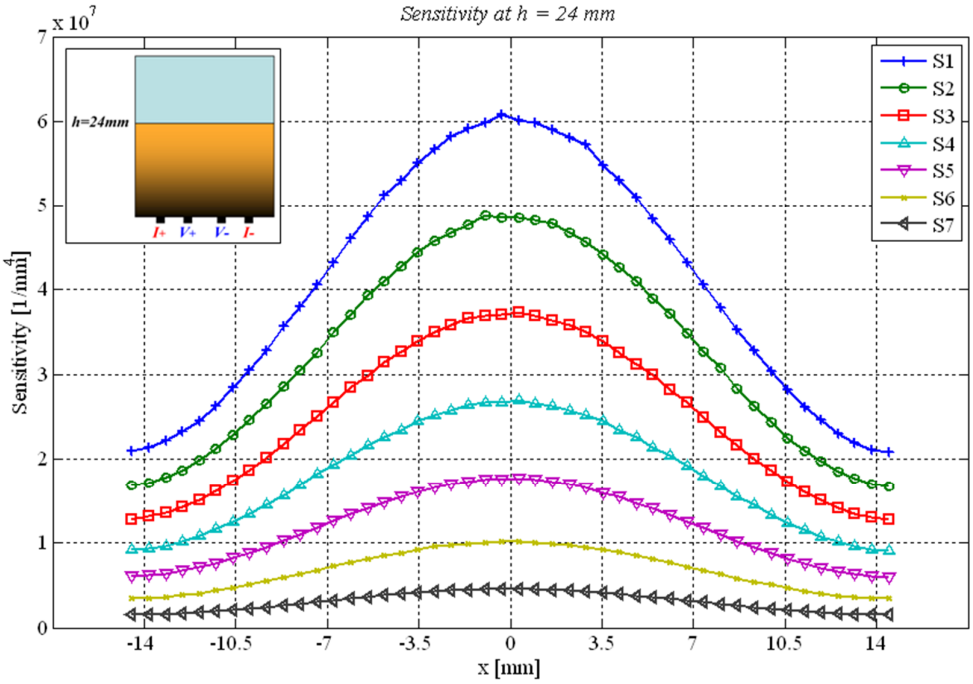


Fig. 11.d. Maximum sensitivity at *h*=24mm for every electrode step.

Fig. 12. Experimental setup. Solartron 1250/1287 system. At the left side of the picture the MEA platform is measured into a Faraday cage.

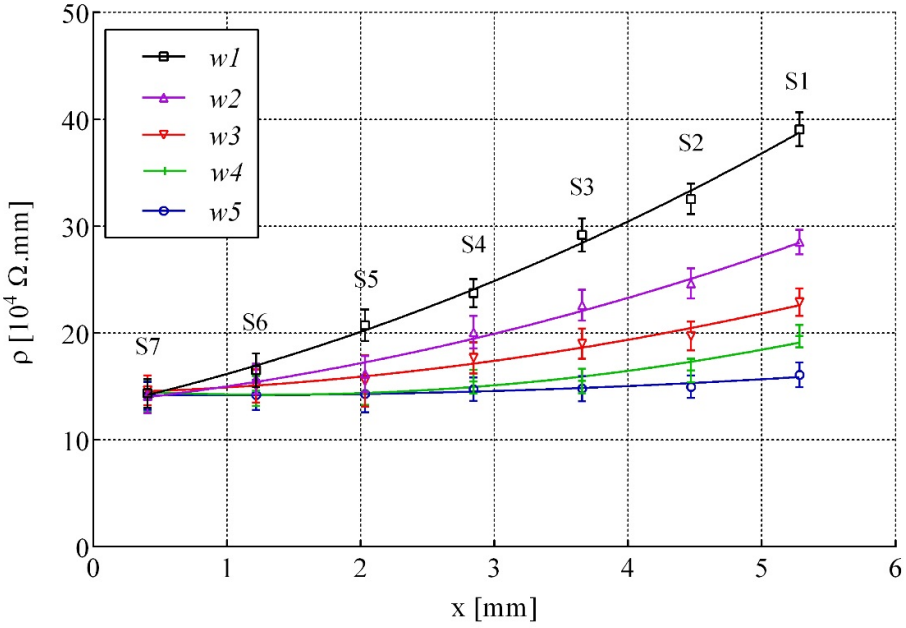


Fig. 13. Apparent resistivity as a function of the electrode spacing for five analyzed samples *w1-w5*.

Table 1. Position of the active electrodes for each step over the *x-axis*, where *x*=0mm in the centre of the array. All units in millimetres.

| Step | $I_+$ | $V_+$ | $V-$ | $I-$ |
|---|---|---|---|---|
| *S1* | *-11.10* | *-3.90* | *3.90* | *11.10* |
| *S2* | *-9.30* | *-3.30* | *3.30* | *9.30* |
| *S3* | *-7.50* | *-2.70* | *2.70* | *7.50* |
| *S4* | *-6.30* | *-2.10* | *2.10* | *6.30* |
| *S5* | *-4.50* | *-1.50* | *1.50* | *4.50* |
| *S6* | *-2.70* | *-0.90* | *0.90* | *2.70* |
| *S7* | *-0.90* | *-0.30* | *0.30* | *0.90* |

Table 2. Layers and thicknesses for the five samples. All units in millimetres.

| | *w1* | *w2* | *w3* | *w4* | *w5* |
|---|---|---|---|---|---|
| $h_t$ | *27.50* | *26.50* | *25.00* | *23.75* | *22.50* |
| $h_w$ | *2.50* | *3.75* | *5.00* | *6.25* | *7.50* |